Available online at www.sciencedirect.com
SCIENCE DIRECT®
Precision Engineering 27 (2003) 382–394
PRECISION ENGINEERING
www.elsevier.com/locate/precision

Linear motion carriage with aerostatic bearings preloaded by inclined iron core linear electric motor

Alexander Slocum*, Murat Basaran, Roger Cortesi, Anastasios John Hart

Massachusetts Institute of Technology, Room 3-445, 77 Massachusetts Avenue, Cambridge, MA 02139, USA

Received 9 July 2002; received in revised form 4 March 2003; accepted 4 March 2003

Abstract

A fundamentally precise and simple linear motion axis design is discussed where the attractive force from the linear motor is used to preload a carriage supported by six rigidly attached porous carbon air bearings. The air bearings are assembled by vacuuming the pads to two orthogonal planes, positioning the carriage above the pads, and then injecting epoxy between the bearings and the carriage. Control of flatness tolerances of the bearings and planes permits over-constraint of the carriage by the bearings, which leads to a high degree of accuracy and moment load capacity via elastic averaging. Good dynamic stiffness is also obtained because of large bearing area and squeezed-film damping. The two orthogonal planes represent an accurate and cost effective geometry that can be created to guide linear motion; and by placing the open-face iron-core motor at the desired position and angle with respect to the bearings, preload forces with equal or otherwise desired relative magnitudes are obtained. Because the attractive force is typically 3–5 times the axial force generated by the motor, the system is inherently stable even in the presence of large externally applied moments that might otherwise induce excessive pitch, yaw, or roll errors.

Keywords: Linear motor; Air bearings; Preload; Elastic averaging; Squeezed-film damping

1. Introduction

Linear motion axes are ubiquitous in manufacturing systems, where for high speed or high accuracy systems, rolling element bearings or pressurized fluid bearings are most often used. To reduce cost and increase simplicity, open-face iron-core linear motors are desirable for high-speed systems, but they can cause excessive loading and premature failure of rolling element bearings. Fig. 1 illustrates a concept for a fundamentally precise and simple linear motion axis where the attractive force from the linear motor is used to preload a carriage supported by air bearings, although this arrangement could also preload other types of bearings depending on the application. The six air bearing pads are assembled by vacuuming the pads to two orthogonal planes, positioning the carriage above the pads, and then injecting epoxy between the bearings and the carriage. The result is accurate and rigid support of the carriage achieved by elastic averaging. In addition, the large bearing areas and small gaps provide squeezed-film damping so good dynamic stiffness is achieved.

A pair of orthogonal planes is a very accurate and low cost geometry that can be used to guide linear motion. By placing the motor at a desired position and angle with respect to the air bearing pads, a desired distribution of preload forces can be obtained on the pads; hence, when a new machine is designed, the preload can compensate for large static weight distributions. Because the attractive forces are typically five times the axial force from the motor, the system is inherently stable even in the presence of externally applied forces and moments. This concept can also be used with angular motion axes, particularly where partial rotary motion is required, as shown in Fig. 2. An advantage of this type of design is that it can be rapidly assembled from modular components.

In a sense, the evolution of this concept started in the early 19th century when Joseph Whitworth championed the three-plate scraping method and described “the vast importance of attending to the two great elements in constructive mechanics, namely a true great plane and the power of measurement” [1]. Accordingly, for many years vee- and flat ways and then double vee-ways used gravity to preload machine tool carriages [2]. Later, James Bryan of LLNL championed the use of DC direct drive motors for friction drives [3], and Anwar Chitayet, the founder of Anorad Corp., unwrapped DC rotary motors into linear electric motors for direct drive of machine tool axes [4]. Meanwhile, Rasnick at ORNL developed a robust method for manufacturing porous carbon air bearings for machine tools [5], which

* Corresponding author. Tel.: +1-603-253-0012; fax: +1-603-224-5369.
E-mail address: slocum@mit.edu (A. Slocum).

0141-6359/$ – see front matter © 2003 Elsevier Science Inc. All rights reserved.
doi:10.1016/S0141-6359(03)00037-0

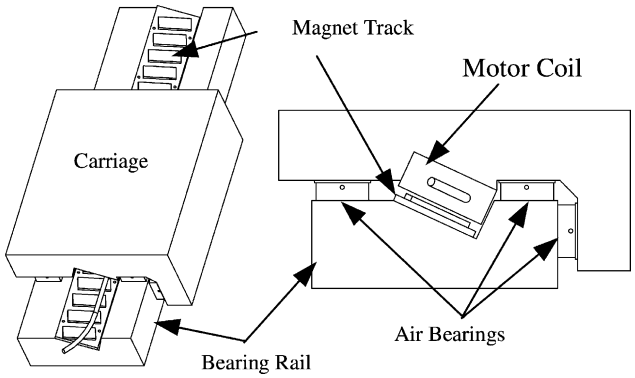

Fig. 1. Motor-preloaded-bearing concept where an iron-core open-face linear electric motor's permanent magnets are used to preload aerostatic bearings.

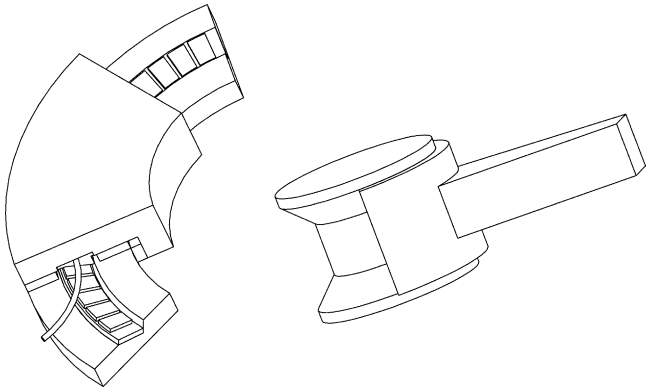

Fig. 2. Motor-preloaded-bearing angular motion design concepts where fundamentally the rotor is an arc segment. Left view shows an iron-core open-face rotary electric motor's permanent magnets are located on a conical surface and used to preload aerostatic bearings. Right view shows conical bearings with magnets that would be on a cylindrical surface.

Devitt of NewWay Bearings Inc. evolved to offer modular off-the-shelf bearings.[1]

In the late 1980s, Van Deuren from Philips Corp. created a kinematic arrangement of five air bearing pads mounted on hollow stems connected to air supply ducts integrated with an extruded carriage structure, and preloaded with an open-face linear electric motor [6]. Because of its robust kinematic design, this design would only require modest accuracy of the flat bearing surfaces; however, the five bearing pads on ball joints would limit the ability of the carriage to resist heavy external moment loads. An example of application of this arrangement is for high speed shuttles in semiconductor manufacturing equipment. However, such kinematic arrangements of air bearings on pivot joints, which allow the carriage to run on what might not otherwise be a straight enough surface, may not provide sufficient tilt stiffness and damping for a carriage that must withstand heavy external machining loads.

Meanwhile, Devitt and Slocum [7] developed a method for vacuuming fluidstatic bearings to flat bearing rail surfaces, positioning and aligning a carriage atop them, and then injecting epoxy to accurately and rigidly anchor the bearings to the carriage. They used this method to create hydrostatic bearing-supported carriages in a classic format where the carriage supported by modular fluidstatic bearings wrapped around the bearing rails. The first machine of this type was an all-ceramic structure grinding machine with modular self-compensating water hydrostatic bearings [8]. Devitt also used this method with porous air bearings he supplied for many different types of machines. The next advance used this method to make the bearings a rigid integral part of a carriage, but instead of using a wrap-around design for preloading them, an inclined, open-face, iron-core, linear electric motor was used. With six bearings rigidly anchored to support the linear motion carriage, the system was over-constrained, but allowably so because of the easily attained accuracy of the two flat planes. This gave the carriage very high pitch, yaw, and roll stiffness [9,10] and the ability to resist heavy external moment loads such as encountered when machining.

A key element of any fluid film bearing is that large areas and small gaps results in a large amount of squeezed-film damping, which is inversely proportional to the third power of the bearing gap. On the other hand, bearing stiffness is inversely proportional to the gap; hence combined with the mass of the system, dynamic performance can vary widely, and it is impractical to generalize on what is the optimal bearing gap. It has been proposed that machine performance can be optimized in real time by dynamically controlling the bearing pad position and/or the bearing gap. For example, spindle designs have been tested that use piezoelectric actuators to radially adjust the position of fluidstatic bearing pads supported by flexures [11] which in effect controls spindle error motion and also can affect the bearing gap. With this design, dynamic radial motion of a spindle at 1000 rpm can be reduced by 50%. Liquid bearings do not suffer from pneumatic hammer caused by excessive volume downstream of the restrictor, and though this enables control of the pressure in the bearing pocket using a servo valve [12–14], it leads to increased cost and complexity. A compromise is a diaphragm type restrictor, where the inlet flow resistance is made proportional to the flow using a diaphragm [15].

Devitt of New Way Bearings uses a hybrid approach,[2] where porous carbon bearings physically contact the rail surface, while providing air pressure to counteract most of the static force the bearings must support. In this method, the effect of the gap is essentially eliminated, but the system does require a high mechanical impedance actuator, such as a ballscrew, to overcome the static friction that is present.

Bearing supply pressure affects the gap, which affects the system damping, which in turn may affect the process for which the machine is used. As discussed later in Section 3, if the supply pressure is too high, chatter can occur in a grinding application. It is therefore likely that as this machine design evolves, supply pressure can be controlled in a quasi-static

[1] www.newwaybearings.com.

[2] Unpublished work, New Way builds and sells such systems, and the results appear promising. See http://www.newwaybearings.com.

fashion: The machine tool controller can change the supply pressure according to process requirements. Output-filtered accelerometers could also be used to sense the onset of chatter and accordingly adjust the supply pressure. In either case, changing the supply pressure will change the bearing gap, which will change the tool offset; therefore, the machine controller would need to incorporate either real time measurement of the gap (expensive) or the use of a look-up table to compensate.

Accordingly, this paper describes the design process and analytical methods used to design a grinding machine based on the motor-preloaded-bearing principle as it has evolved to this day: the rigid attachment of six aerostatic bearings to a carriage such that its motion accuracy and stiffness on two orthogonal precision planes is enhanced by elastic averaging, and it is preloaded by the attractive forces from an iron core linear electric motor.

2. Design analysis

Porous graphite bearings were selected for the design because they are very damage resistant. Static performance of porous carbon air bearings can be predicted [5], and for commercially available bearings, design data (bearing gap as a function of area, pressure, and force) is typically directly obtained from the manufacturer as shown in Fig. 3. Table 1 shows data taken from Fig. 3 and analyzed to give the observed efficiency η which is obtained from stiffness $= \eta \times$ area $\times P_{\text{supply}}/(\text{gap}/2)$. The bearings have an "optimal" design region where the gap (lift) is 6–15 μm. When the supply pressure is increased, the stiffness decreases because the gap increases for a given load, and the damping ζ also decreases. Curves were fit to the data for these bearings at 4 bar supply pressure to provide design estimates for the gap, given the applied load, and the resulting stiffness:

$$\begin{aligned} F_{50\times100} &= 0.0065h^4 - 0.496h^3 + 14.598h^2 \\ &\quad - 223.351h + 1937, \\ F_{75\times150} &= 0.0394h^4 - 2.515h^3 + 61.32h^2 \\ &\quad - 786.5h + 5306.3 \end{aligned} \tag{1}$$

$$\begin{aligned} h_{50\times100} &= 8.0046 \times 10^{-12}F^4 - 3.583 \times 10^{-8}F^3 + 6.937 \\ &\quad \times 10^{-5}F^2 - 0.0751F + 39.725, \\ h_{75\times150} &= 1.271 \times 10^{-13}F^4 - 1.096 \times 10^{-9}F^3 + 4.852 \\ &\quad \times 10^{-6}F^2 - 0.0149F + 24.312 \end{aligned} \tag{2}$$

$$\begin{aligned} K_{50\times100} &= -0.0258h^3 + 1.489h^2 - 29.196h + 223.35, \\ K_{75\times150} &= -0.158h^3 + 7.543h^2 - 122.644h + 786.51 \end{aligned} \tag{3}$$

There are numerous references for calculating the squeezed-film damping coefficient, particularly for thin gas layers, many of which have been motivated by the design of MEMS structures seeking ever higher quality factors Q [16]. Much of the analysis of squeeze films for MEMS devices is based on early work for hydrostatic fluid bearings. However, specific reference for a formula for estimating the

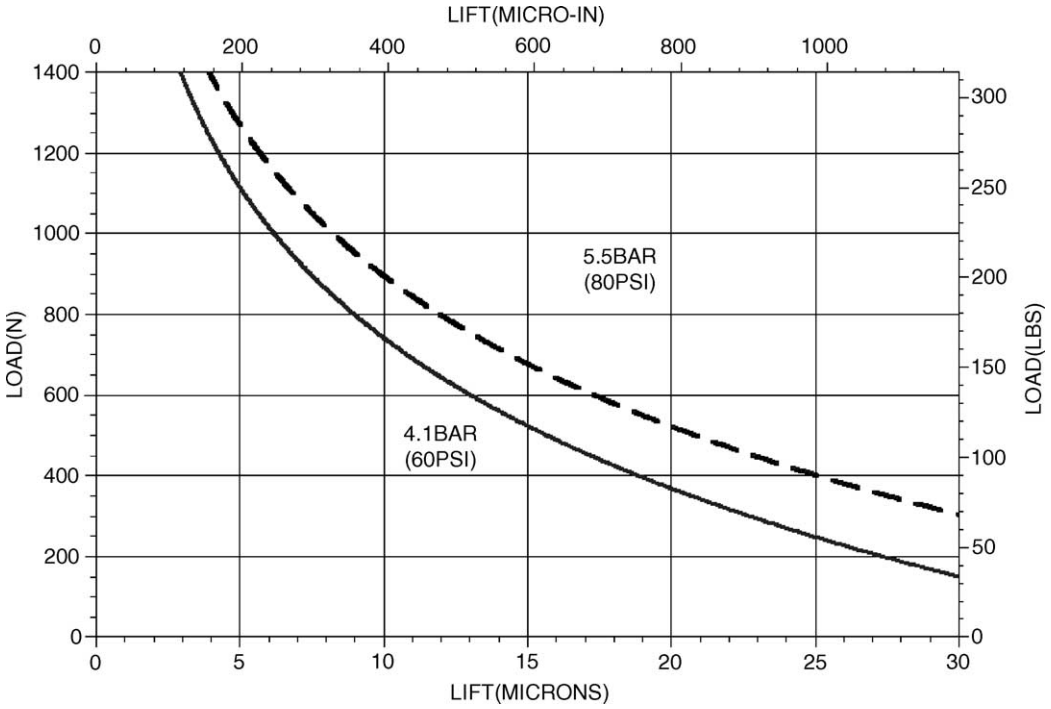

Fig. 3. Load vs. gap height and pressure for 50 mm × 100 mm commercially available porous graphite air bearing pad (www.newwaybearings.com).

Table 1
Bearing performance data for 50 mm × 100 mm commercially available porous graphite air bearing pad, derived from Fig. 3 (www.newwaybearings.com)

Load (N)	Lift (μm)		Stiffness (N/μm)		Efficiency, η		h_4/h_5 (gap)	k_4/k_5 (stiffness)	ζ_4/ζ_5 (damping)
	Supply pressure (atm)								
	4	5							
400	18.5	25.0	22	16	0.19	0.15	1.4	1.4	2.5
500	15.5	21.0	33	25	0.25	0.20	1.4	1.3	2.5
600	13.0	17.5	40	29	0.25	0.19	1.3	1.4	2.4
700	11.0	14.5	50	33	0.27	0.19	1.3	1.5	2.3
800	9.0	12.0	50	40	0.22	0.19	1.3	1.3	2.4
900	7.5	10.0	67	50	0.24	0.19	1.3	1.3	2.4
1000	6.3	8.5	80	67	0.24	0.22	1.4	1.2	2.5
1100	5.0	7.0	80	67	0.19	0.18	1.4	1.2	2.7
1200	3.8	5.5	80	67	0.15	0.14	1.5	1.2	3.2

squeezed-film damping of rectangular porous air bearings was not found, and it was not feasible at this stage to create a detailed analytical model or conduct a numerical simulation. Since it is empirically known that the bearings can be well damped, and the pores feed the gas at all points, an experiment was done to see if the known equations for estimating the squeezed-film damping between solid plates could be used as a design engineering tool for the porous air bearings. The damping coefficient b (N/m s) for a rectangular plate bearing of width w (shorter dimension), and length L (longer dimension), gap h, and fluid viscosity μ is determined from the pressure distribution under a plate subject to a sudden vertical downward motion toward a stationary substrate. Senturia [17] solved the Reynolds equation in the gap under a long slender plate ($L \gg w$), giving:

$$b_{L\gg w} = \frac{96\mu_{\text{eff}} L w^3}{\pi^4 h^3} \tag{4}$$

$$\mu_{\text{eff}} = \frac{\mu}{1 + 9.64(\lambda/h)^{1.159}} \tag{5}$$

The effective viscosity μ_{eff}, which accounts for slip flow in very small gaps, is determined by Veijola [18] based on the fluid mean free path λ. The value of λ is about 0.1 μm for air, reducing the viscosity by about 10% at typical bearing conditions.

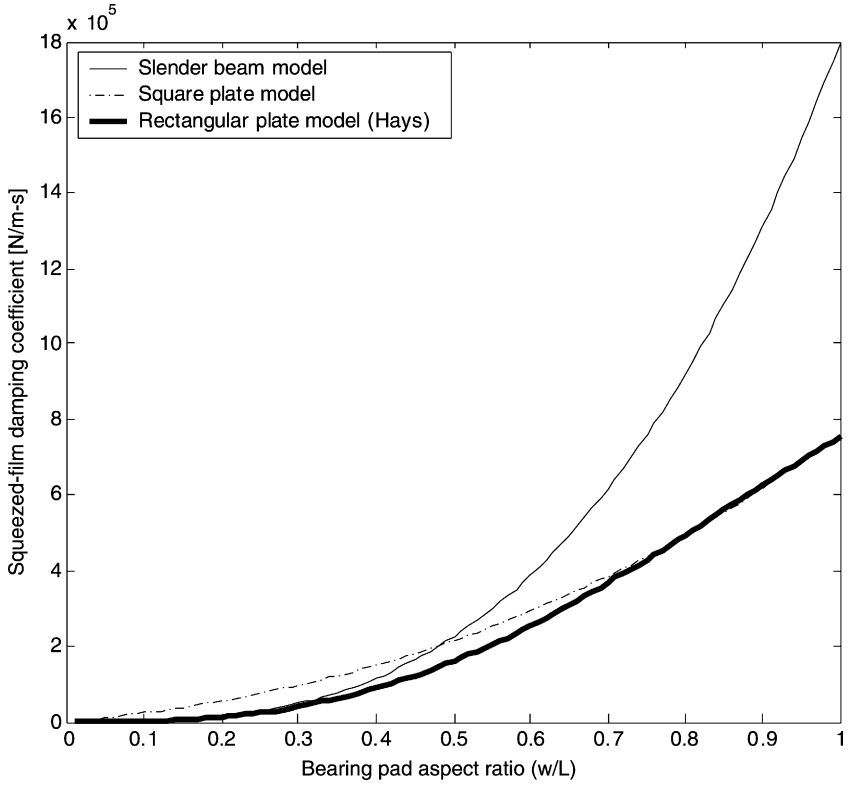

Fig. 4. Squeezed-film damping coefficients predicted by slender plate, square plate, and rectangular plate models.

The solution for a long slender plate is a one-dimensional model, where the flow only squeezes out under the long edge of the plate. However, the flow under a truly rectangular plate seeps from all four edges. Following Senturia and solving the Reynolds equation in two dimensions for a square plate gives:

$$b_{L\cong w} = \frac{32\mu_{\text{eff}} wL(w+L)^2}{\pi^5 h^3} \tag{6}$$

This assumes that the plate length and width are approximately equal, so the same amount of flow is lost out of each side edge.

Alternatively, Hays [19] develops a series solution for damping of a rectangular plate, exactly modeling the pressure distribution under the plate. Fitting a curve to values of Hays' solution tabulated by Fuller [20], the expression for b of a rectangular plate is of the same form as the slender plate solution, but the leading constant depends on the aspect ratio (w/L) of the plate:

$$b = K_s \frac{\mu_{\text{eff}} w^3 L}{h_o^3} \tag{7}$$

$$K_s = 0.991 - 0.578 w/L,\ w/L \le 1 \tag{8}$$

Fig. 4 shows the damping coefficients predicted by each model as the plate aspect ratio varies from $w/L = 0.001$ to $w/L = 1$ (specifically for $L = 0.1$ m and $h = 9\,\mu$m). The slender plate model agrees with Hays' solution for $w/L < 0.3$, while the square plate model agrees with Hays' solution for $w/L > 0.75$. Between these limits, both the slender plate and square plate models predict damping values greater than the exact solution, so the curve fit to Hays' solution is recommended as a simple model for predicting the damping between parallel plates of any aspect ratio.

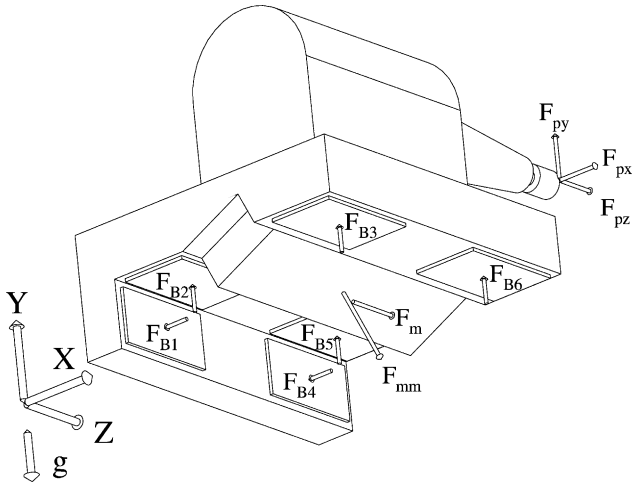

Fig. 5. Generalized forces on the carriage; note that the mass of the carriage and its location (m_c, x_c, y_c, z_c) and the spindle (m_s, x_s, y_s, z_s) are not shown.

Inputs (N, mm) in BOLD, Outpus in RED					
Ps (N/mm^2,p si)	**0.55**	80	Bearing supply pressure		
gap, h (mm)	**0.013**		Nominal bearing gap		
a(m/s^2, g)	**0.1**	0.98	Axis acceleration		
gravity, g	**9.8**				
bearing efficiency, eta	**0.2**				
Bearing 1		**Bearing 2**		**Bearing 3**	
A_1(mm^2)	**11250**	A_2	**5000**	A_3	5000
K_1(N/mm)	190385	K_2	84615	K_3	84615
X_1	**50**	X_2	**100**	X_3	**250**
Y_1	**100**	Y_2	**175**	Y_3	175
z_1	**-150**	z_2	-150	z_3	-150
Bearing 4		**Bearing 5**		**Bearing 6**	
A_4	11250	A_5	5000	A_6	5000
K_4	190385	K_5	84615	K_6	84615
X_4	50	X_5	100	X_6	250
Y_4	100	Y_5	175	Y_6	175
z_4	150	z_5	150	z_6	150
Process		**Spindle**		**Carriage**	
Fpx(N)	**20**	Mass ms (kg)	**0**	Mass mc (kg)	**30**
Fpy(N)	**20**	Xs	**200**	Xc	**175**
Fpz(N)	**2**	Ys	**300**	Yc	**200**
Xp	**150**	Zs	**50**	Zc	**0**
Yp	**300**	**Motor**			
Zp	**225**	Magnet preload Fmm (N)		**3800**	
		Kservo (N/mm)		**500000**	
		Xm		**150**	
		Ym		**150**	
		Zm		**0**	
		mount angle theta (rad, deg)		0.524	**30**

Fig. 6. Motor-preloaded-bearing design spreadsheet input parameters.

The value of b can then be combined with the total stiffness and mass of the system to estimate the quality factor (amplification at resonance) Q. For a second-order model of a carriage supported by air bearings, with a total mass m of the carriage and attached components, and total system stiffness k, the second order system damping factor ζ and quality factor Q (η is the % damping) can be determined:

$$m\ddot{x} + b\dot{x} + kx = 0 \quad \ddot{x} + 2\varsigma\omega_n\dot{x} + \omega_n^2 x = 0 \qquad (9)$$
$$\varsigma = \frac{b}{2\sqrt{km}} \qquad Q = \frac{1}{2\zeta\sqrt{1-\zeta^2}} = \frac{100}{\eta}$$

If ζ is greater than 0.7, the system will be critically damped, although in practice it is very difficult to achieve critical damping. This is the source of the misnomer that a system can have too much stiffness; on the contrary, a system can have too little damping. In the case of a magnet-preloaded bearing system, if the supply pressure is increased in the belief that it will yield greater stiffness, as is the case for the bearings preloaded by geometric constraints, the stiffness can actually decrease because of the resulting gap increase. In addition, since the squeezed-film damping coefficient is a function of the gap cubed, the damping will drop significantly. However, as will be discussed in the results, these formulae predict damping values which do not match the experiments, indicating that a damping prediction formula for modular porous air bearings is needed.

In order to obtain the desired effect of preloading the bearings evenly using the linear electric motor's permanent magnets, a simple force balance can be used as shown in Fig. 5. Each force is located at appropriate x, y, z coordinates representing the center of stiffness of the bearing; for example, the coordinates of the center of stiffness of bearing i are x_i, y_i, and z_i. There are six unknown bearing forces and an unknown motor actuation force (F_m). The preload force F_mm provided by the magnets is assumed constant. These seven unknowns can be solved for using force and moment balance about all three axes and a constraint equation requiring bearings 2, 3, 5, and 6 to remain in a plane as they deflect, even though in actuality they are overconstrained.[3] Assuming linear bearing stiffness $\delta_i = F_{Bi}/k_i$, the following equilibrium equations result:

$$[A] = \begin{bmatrix} -1 & 0 & 0 & -1 & 0 & 0 & 0 \\ 0 & 1 & 1 & 0 & 1 & 1 & 0 \\ 0 & 0 & 0 & 0 & 0 & 0 & 1 \\ 0 & z_2 & z_3 & 0 & z_5 & z_6 & -y_\mathrm{m} \\ z_1 & 0 & 0 & z_4 & 0 & 0 & x_\mathrm{m} \\ -y_1 & -x_2 & -x_3 & -y_4 & -x_5 & -x_6 & 0 \\ 0 & \dfrac{1}{k_2(x_2-x_3)} & \dfrac{-1}{k_3(x_2-x_3)} & 0 & \dfrac{-1}{k_5(x_5-x_6)} & \dfrac{1}{k_6(x_5-x_6)} & 0 \end{bmatrix} \qquad (10)$$

$$[B] = \begin{bmatrix} F_\mathrm{mm}\sin\theta + F_{Px} \\ -F_\mathrm{mm}\cos\theta - m_\mathrm{c}g - m_\mathrm{s}g + F_{Py} \\ -m_\mathrm{c}a - m_\mathrm{s}a + F_{Pz} \\ -F_\mathrm{mm}z_\mathrm{m}\cos\theta - m_\mathrm{c}gz_\mathrm{c} - m_\mathrm{s}gz_\mathrm{s} \\ \quad + F_{Py}z_p - F_{Pz}y_p \\ -F_\mathrm{mm}z_\mathrm{m}\sin\theta - F_{Pz}z_p + F_{Pz}x_p \\ -F_\mathrm{mm}x_\mathrm{m}\cos\theta + F_\mathrm{mm}y_\mathrm{m}\sin\theta + m_\mathrm{s}gx_\mathrm{s} \\ \quad + m_\mathrm{c}gx_\mathrm{c} + F_{Px}y_p - F_{Py}x_p \\ 0 \end{bmatrix} \qquad (11)$$

$$[F_{B1}F_{B2}F_{B3}F_{B4}F_{B5}F_{B6}F_\mathrm{m}]^T = -[A]^{-1}[B] \qquad (12)$$

These equations are easily solved using an Excel™ spreadsheet, which makes it convenient to input the design parameters, as shown in Fig. 6. Here it was assumed that the bearing stiffness was equal to the product of the efficiency, bearing area and supply pressure divided by the nominal bearing gap. Note that to accurately predict machine performance, a detailed error budget should be performed [21], or ideally a study of the probabilities of combinations of errors and their net effect on work volume accuracy [22] should be conducted. Fig. 7 shows the outputs, where the spreadsheet's *Solver* function can be used to vary parameters to minimize error motions at the tool point. The effect of varying magnet preload forces could also be studied, as well as the effect on system dynamic performance.

3. Experimental systems

To verify the ease of construction and assembly hypothesis, simple prototypes were built using machined steel rails with carriages supported by cam followers and preloaded by permanent magnets were built. The simple prototypes for linear and angular motion systems are shown in Fig. 8. These simple "sketch" models verified the robustness of the design and the ease with which the systems could be manufactured.

The next step was to build a precision bench level experiment to evaluate the manufacturing process and to determine the effect of the motor's iron core passing over the permanent magnets. The bearing rails were made from granite to ensure that the bearings would not be damaged should they slide across the rails in case something were to drop on them during handling or in the lab; in addition, it was easier to obtain finished granite components. In anticipation of high speed application, and to increase the ease with which the carriages

[3] It is assumed that the porous carbon air bearings, which have been rigidly epoxied in place as opposed to being mounted on swivels like feet, are in effect vast arrays of springs and since they must comply with the same flat surfaces, errors in the bearings and the surfaces will average out by the elastic quality of the air bearings' stiffness as they are preloaded by the motor magnet attraction force.

Deflections at Process Point (microns, microradians)				
	Process only	Mass, Accel.	Angular	
δx	0.466	-0.12	Pitch (ε_x)	0.001
δy	0.242	-1.00	Yaw (ε_y)	-0.001
δz	-0.12	0.07	Roll (ε_Z)	-0.002

Results of Bearing Force and Deflection analysis											
All Loads				Preload only				Process Forces only			
Forces (N)		Defl. (microns)		Forces (N)		Defl. (microns)		Forces (N)		Defl. (microns)	
FB1	960	1	-5.04	FB1	950	1	-4.99	FB1	-5	1	0.03
FB2	833	2	-9.85	FB2	780	2	-9.22	FB2	-13	2	0.15
FB3	948	3	-11.21	FB3	865	3	-10.22	FB3	17	3	-0.20
FB4	960	4	-5.04	FB4	950	4	-4.99	FB4	25	4	-0.13
FB5	834	5	-9.86	FB5	780	5	-9.22	FB5	-27	5	0.32
FB6	949	6	-11.22	FB6	865	6	-10.22	FB6	3	6	-0.04
Fm	27	dservo	-0.05	Fm	0	dservo	0.00	Fm	-2	dservo	0.00

Location of Pitch, Yaw, Roll Axis					
Pitch Axis		Yaw Axis		Roll Axis	
		Xya	50	Xra	175
Ypa	175			Yra	175
Zpa	0	Zya	0		

Deflections (microns, microradians) at approximate center of stiffness											
Mass, Acceleration, Process				Preload Only				Process Only			
δx	0.05	Pitch (ε_x)	0.000	δx	4.990	Pitch (ε_x)	0.000	δx	0.053	Pitch (ε_x)	0.001
δy	-0.81	Yaw (ε_y)	0.000	δy	-9.723	Yaw (ε_y)	0.000	δy	0.059	Yaw (ε_y)	-0.001
δz	-0.05	Roll (ε_Z)	-0.002	δz	0.00	Roll (ε_Z)	-0.007	δz	0.00	Roll (ε_Z)	-0.002

Fig. 7. Motor-preloaded-bearing design spreadsheet outputs.

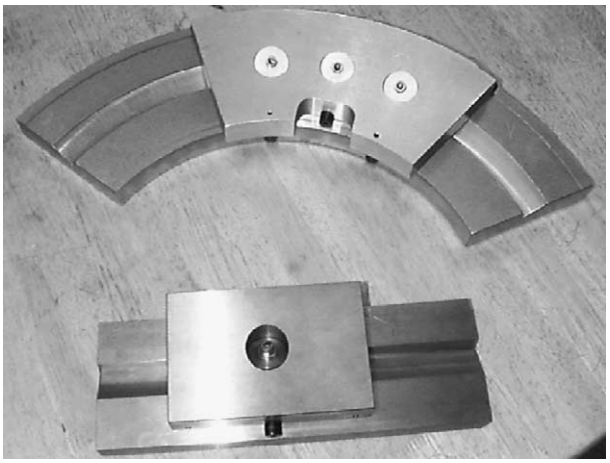

Fig. 8. Proof-of-concept "sketch" models for linear and angular motion concepts.

could be moved around the lab, the carriages were cast from magnesium. For a precision machine tool, however, a magnesium carriage would require even tighter temperature control than usual.

The bearings were installed by holding them to the granite rail surfaces using vacuum, and then the carriage was placed over them and held so its precision surfaces were parallel to the rail using fixtures as shown[4] in Figs. 9 and 10. Then, the proper motor gap was set with a shim. Epoxy was then injected in the region between the backs of the bearings and the pockets within the carriage. After the bearings were potted in place with epoxy, the air supply was turned on, the carriage rose, and the shim was removed.

3.1. Bench level experiment results

The Bench level prototype carriage was made from a magnesium casting, as shown in Fig. 10, and had a mass of 20 kg. Fig. 11 shows the average carriage displacement for various supply pressures when the air is turned on, and for different loadings applied by adding weights to the center of the carriage. The measured nominal gap of 9 μm at 0.4 N/mm^2 (60 psi) indicates from Eqs. (1)–(3) a stiffness of 62 N/μm per bearing at a total load per bearing of 800 N to 123 N/μm per bearing at a total load per bearing of about 1200 N. Apparently, although the magnesium carriage was light, for the initial intended application of shuttling silicon wafers, its low modulus allowed for greater-than-desirable deflections under heavy external point loads. Looking ahead to the measurements of natural frequency shown in Table 2, with a measured frequency of 607 Hz, and a mass of 20 kg, the carriage stiffness is calculated to be 291 N/μm for the mode corresponding to vertical bearing deflection. This is in general agreement with the predicted stiffness values. The average measured carriage stiffness values,[5] on the other hand, were

[4] The original thought was to make modular "L" shaped elements that could then be bolted together to form a small machining center.

[5] It should be noted that one of the bearings had less than half the deflection than the others. The air lines were checked and it did not appear that there was any restriction, and it was unlikely that the bearings themselves had significantly different porosity; thus, when the next system is constructed, the bearings will be evaluated individually prior to installation.

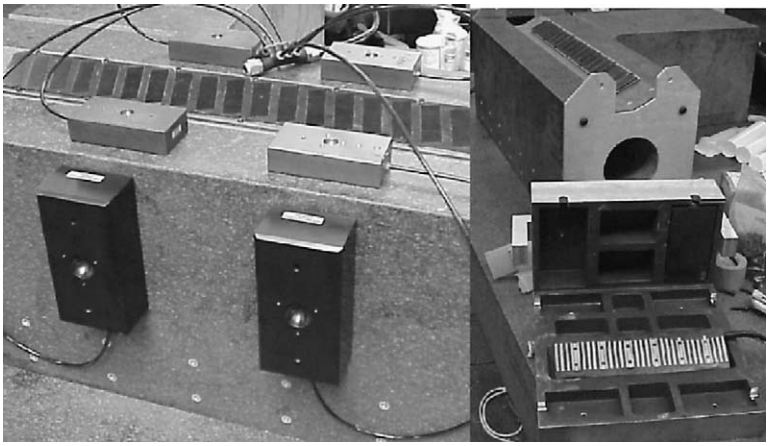

Fig. 9. Bench level prototype components prior to assembly.

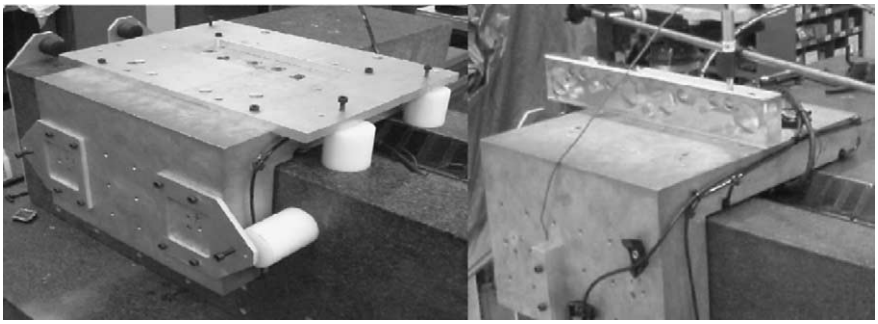

Fig. 10. Bench level prototype system with bearings being replicated in-place, and during metrology tests.

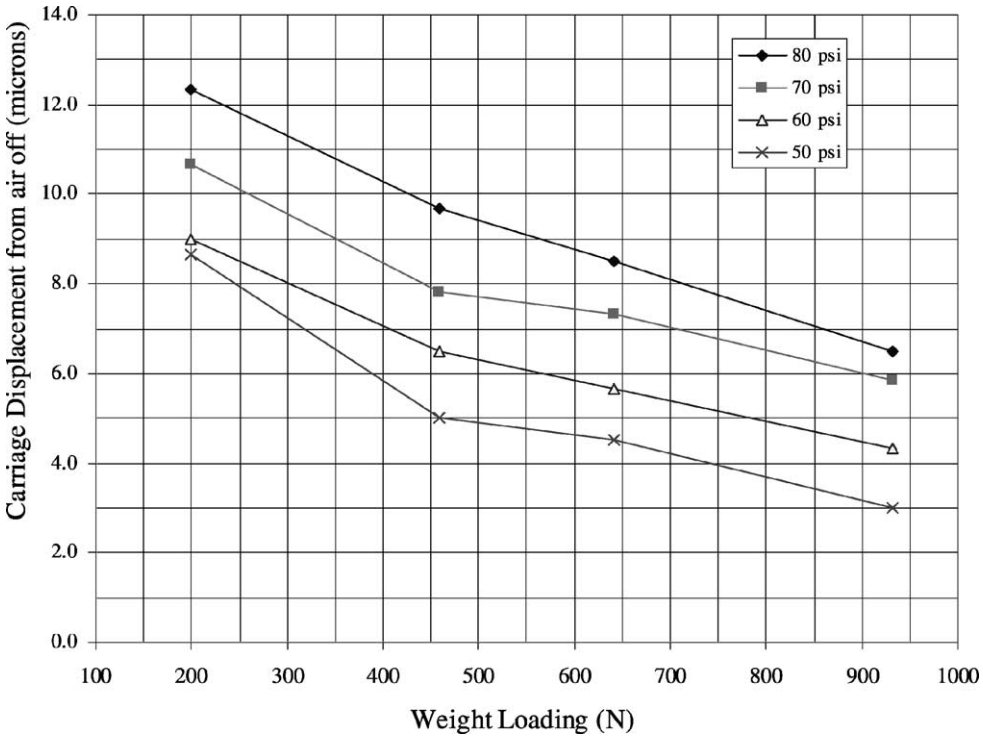

Fig. 11. Average displacement of the carriage when the air is turned on.

Table 2
Experimental modal analysis on the bench level experiment system

Frequency (Hz)	Damping η (%)	Q	Mode shape
Air on (4 atm supply)			
362	3.8	26	Twisting
487	1.9	53	Carriage spreading like a "hinge"
607	3.3	30	Main carriage mode with center oscillating in Z
Air off			
501	1.3	77	Whole carriage moves up and down in Z
1430	0.6	167	Top center of carriage oscillating

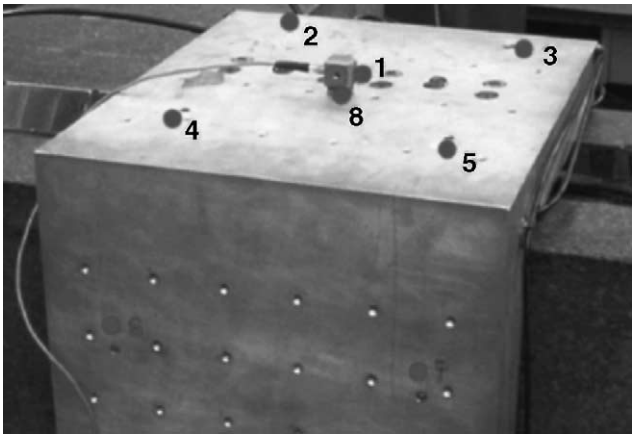

Fig. 12. The carriage and the 8 points used for modal analysis. Point 1 is the impact point, and Points 2–7 are the measurement points.

125 N/μm at 80 psi, 151 N/μm at 70 psi, 157 N/μm at 60 psi, and 129 N/μm at 50 psi. It is not unusual for a machine tool's structure stiffness to be on the order of the stiffness of the bearings, and hence, these values seem reasonable.

Experimental modal analysis was conducted on the system to address concerns that magnet preloaded air bearings (i.e. a carriage not supported by "wrap around" preloaded bearings) might not be damped well enough for machining applications. Fig. 12 shows the experimental modal analysis test points, and Fig. 13 shows typical frequency response functions obtained at the center of the carriage with the air on and off. This shows that the modes seen with the air on are very much dependent on bearing performance. Table 2 summarizes the modal data. In particular, note that the damping of the 3rd mode (607 Hz, where the carriage moves perpendicular to the rail) is 3.3%. On the other hand, Fig. 14 shows output from the design spreadsheet that uses the simple squeezed-film damping relations given in Eqs. (7) and (8). The measured damping is respectable, better than for typical rolling element bearings and not as good as for hydrostatic bearings; however, it is far from the predicted values.

It is interesting to consider the effect of the compressibility of the air film on the damping equations. If we assume no temperature effects and no additional leakage out the side of the pad during the dynamic excitation, which is probably reasonable given the large area/gap in this case, then from starting with $P_1V_1 = P_2V_2$, an estimate of the stiffness of the air column is simply:

$$K_{\text{air}} = \frac{wLP_{\text{gap pressure}}}{h} \tag{13}$$

However, if the air film compressibility had the effect of lowering the effective stiffness of the system, then the damping value ζ would actually increase as given by Eq. (9). If we take as a starting point the damping predicted by Eqs. (6) and (7), shown in Fig. 14 to be far greater than critical damping, and increase the stiffness K to yield a damping value observed in the experiments, then K would have to be over 100,000 times greater. Eq. (13), however, yields stiffness values that are essentially equal to the aerostatic stiffness of the bearing. Thus, clearly the issue seems to be the model for how air is being

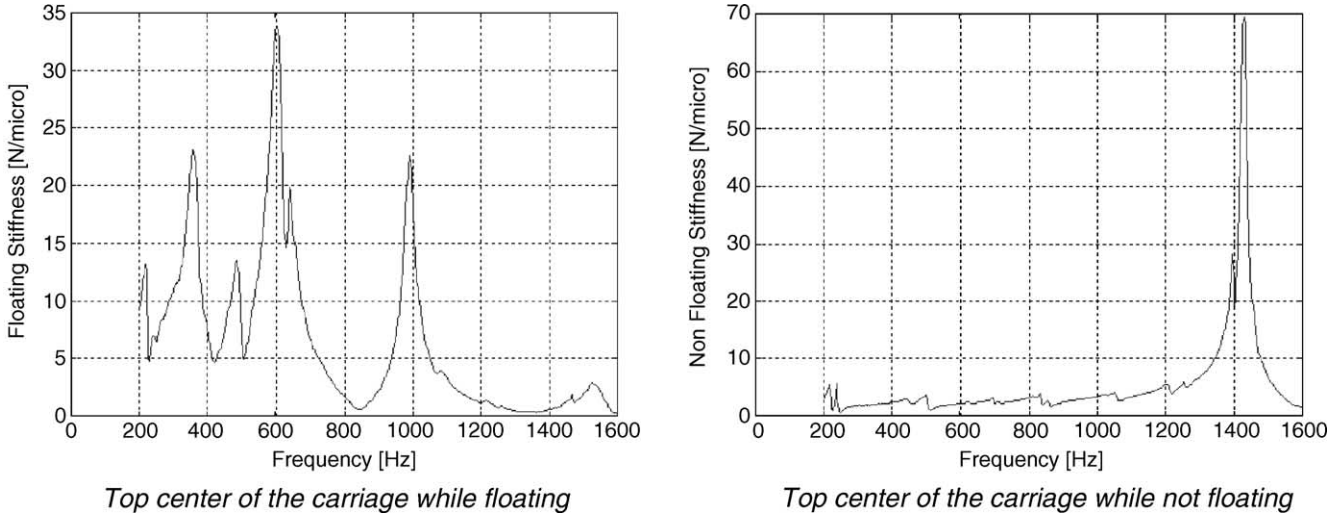

Fig. 13. Frequency response functions for the center point (point 8) of the carriage with the air on and the carriage floating (left) and the air off (right).

Estimated System Dynamics (squeeze film damping)		
Supply pressure (N/mm^2)	**0.4**	
Number of bearing pads	**4**	
Bearing width, w (mm)	**50**	
Bearing length, L (mm)	**100**	
Air viscosity, mu (N-s/m^2)	**1.84E-05**	
Knudsen number	**1.11E-02**	
Corrected air viscosity (N-s/m^2)	**1.75E-05**	
gap (mm)	**0.009**	
Ks	**0.702**	
Total mass, m (kg)	**20**	
Measured first mode (Hz)	**607**	
Frequency predicted carriage stiffness, k (N/micron)	**291**	
Equation predicted carriage stiffness, k (N/micron)	**222**	
	Full plate	Reduced plate
Predicted natural frequency (Hz)	531	531
w and L reduction factor for porosity		**4.4**
corrected bearing width		**11.31**
corrected bearing length		**22.62**
Damping, b (N/(m/s)	842024	2205
Damping factor, zeta	6.315	0.017
Quality (dynamic amplification) factor Q	**N/A**	30.2
Percent damping	**N/A**	3.3%

Fig. 14. Estimated carriage dynamic performance for the main carriage vertical translation mode.

squeezed out of the gap. Accordingly, it is hypothesized that the squeeze film pressure is not as predicted by the model for solid plates, and instead some of the air is being forced back through the porous surface.

As a very rough estimate to test this hypothesis, Fig. 14 shows how a correction factor is used to scale the width and length of the bearing to see what size bearing would yield the observed damping, given the stiffness of the actual bearing. Squeezed-film damping from a 11 mm × 22 mm flat plate combined with the stiffness from the 50 mm × 100 mm porous carbon air bearing yields the observed damping of the system. It is interesting to note that in general, for compensated bearings the flow resistance into the bearing is on the order of the flow resistance out of the bearing. Thus, if we assume that for a porous bearing each gas molecule has the option of traveling all the way to the bearing perimeter, or back through

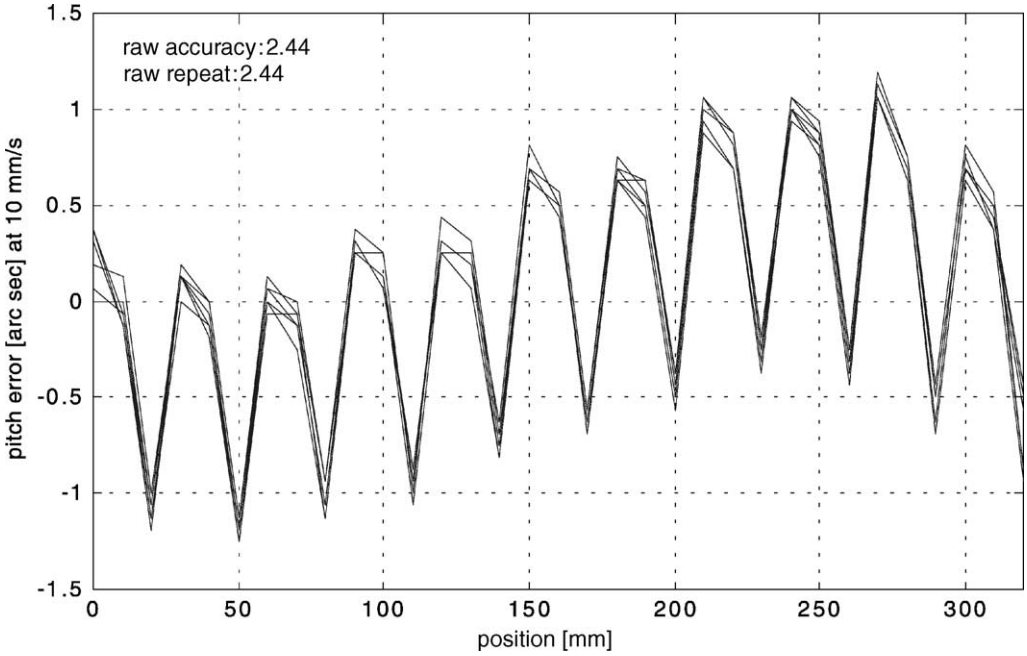

Fig. 15. Pitch motion of the carriage; the period is equal to the magnet pitch.

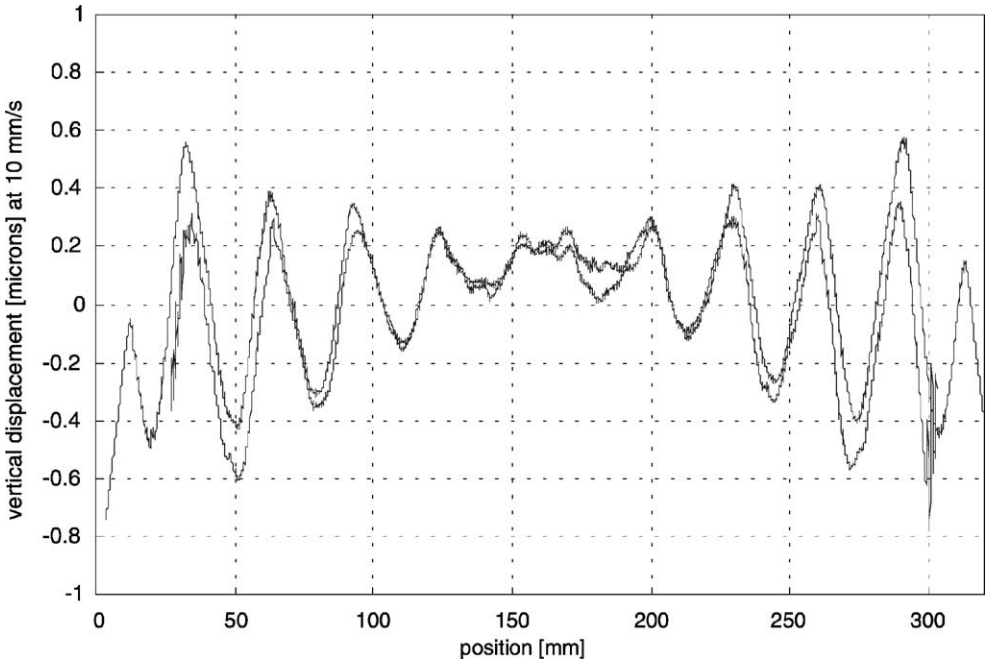

Fig. 16. Straightness measurements taken with a moving straightedge as shown in Fig. 10; hence, straightness includes product of pitch error and axial distance from center of carriage.

a local pore, it seems reasonable that the effective damping area is only a fraction of that of the actual bearing. Numerical simulations of damping of perforated MEMS structures, such as those presented by Veijola and Mattila [23] provide insight into this effect. Hence, we conclude that a damping model of the porous carbon bearing should include not only the classic squeezed-film effects, but also the effects of backflow through the pores; and further research will be required to develop an engineering formula for predicting the damping coefficient for porous flat pad air bearings.

With respect to error motion measurements, the pitch, measured as shown in Fig. 15 using a laser interferometer and a moving straightedge, was found to be a respectable ± 1 arc second over 300 mm of travel, with repeatability on the order of 1/4 arc second. For better performance, two motor coils or additional iron could be spaced apart to balance forces and reduce pitching moments. The straightness was also measured using a moving straightedge and the results are shown in Fig. 16. In the center, where there is no pitch component, the straightness is on the order of 0.3 μm, which is the tolerance of the granite surfaces.

4. Manufacture and testing of the bench level prototype grinder

Spindles were mounted to the test carriages to create the Bench level prototype Grinder, shown in Fig. 17, to deter-

Fig. 17. Bench level prototype system.

Fig. 18. Test parts ground on the bench level prototype system. Part: roller bearing inner ring; material: AISI 52100; hardness: 57–62 Rc; maximum stock removal: 0.300 mm on diameter. Required process: grind the bore diameter and maintain 0.4 Ra or better surface finish and 0.005 mm or less taper and straightness. Incoming part condition: back face (locating surface) and OD were ground.

mine if the linear motor driven axes could be servo controlled to produce coordinated motion suitable for grinding. In order to set up the servos, the two identical axes from the bench level experiments were placed on an available wooden workbench so their actuators, encoders, and spindles could be connected to the servo amplifiers and the PC-based machine tool controller.

A MachineMate^{TM} MM1 PC-based controller was installed with position feedback from Heidenhain LS403 and Renishaw RGH22 tape-type encoders which had A&B quadrature output (5 V TTL). The actuators were Anorad LCK-2 open-face linear motors, connected to Ultra 3000^{TM} Allen-Bradley servo amplifiers. Current and velocity loops were closed within the servos, while the position was closed using the PC controller. The system integrated with the electronics was actually ready long before a base was to become available; hence, it was decided to proceed and rough ID grind the sample parts shown in Fig. 18. The results for this quickly assembled system, as shown in Table 3, are actually quite reasonable given that the modular axes were placed on a maple wood workbench.

The part was clamped by a collet chuck, which was ground in place on the spindle. The work spindle was driven by a belt drive motor at 600 rpm (approximately 0.8 m/s surface speed) and the grinding spindle had a resin bonded vitrified grinding wheel (20 mm diameter and the length was equal to the part length); and was belt driven at 30,000 rpm (31 m/s surface speed). The grinding process was done by using a "dress before finish" and oscillating grinding method during rough and finish grinding. Rough grinding was done with a fast feed rate (0.005 mm/s oscillating at 8 Hz) until 0.050 mm of stock was left to the finish size. The grinding wheel was then dressed with a single point diamond and started for finish grinding the remaining stock. At the end of the finish grind the grinding wheel was allowed to spark out for 6 s. The coolant was a 5:1 water/oil mixture and the pressure was 2 bar.

The process was very smooth and quiet which meant the wheel was cutting free and the feed rate could be increased for more aggressive grinding. However, the clamping system was not strong enough and the part became loose when the feed rate was increased. Therefore, it was not possible to optimize the grinding cycle to minimize cycle time. However, the machine was stiff enough to grind a part chatter-free and remove stock better than a similarly sized and equipped production machine. It should be noted that as anticipated, when the bearing supply pressure was increased by several bar, chatter was encountered; hence, there is an optimal bearing

Table 3
Roundness and surface finish of rough ground test parts: (1) R1 (reading 1) is at the step end, R2 middle, R3 opposite end; (2) roundness measurement conditions: filter 50 cpr, 3 mm stylus, least squares circle evaluation; (3) surface finish measurement conditions: (6) 0.8 mm cut offs, measured on a S-5 form Talysurf with a 0.2 mm tip radius stylus

Part	Roundness at R1 (μm)	Roundness at R2 (μm)	Roundness at R3 (μm)	Ra at R1 (μm)	Ra at R2 (μm)	Ra at R3 (μm)
1	6.2	6.7	6.6	0.43	0.43	0.62
2	6.1	4.6	5.1	0.47	0.42	0.48
3	11.0	10.1	11.4	0.26	0.31	0.38
4	10.9	10.5	9.5	0.35	0.27	0.27
5	10.9	8.1	7.6	0.51	0.35	0.36
6	8.3	14.9	6.2	0.80	0.49	0.48
7	8.8	7.0	6.4	0.65	0.45	0.43
8	14.2	19.7	17.7	0.73	0.52	0.51
9	18.3	22.3	26.3	0.88	0.52	0.53
10	19.2	22.9	24.5	0.87	0.35	0.43

supply pressure which enables the bearing gap to achieve an appropriate level of damping and hence dynamic stiffness.

5. Conclusions

The machine performed in accordance with predictions, and in particular the principle of using flat planes of sufficient accuracy to enable six bearings to be rigidly mounted to the carriage to achieve an elastic averaging effect and good dynamic stiffness proved to be very successful; however, a more accurate damping model is required that would consider the effects of compressibility and porous media.

The pitch error caused by the magnets was very low, on the order of an arc second, and was repeatable to 1/4 arc second. Note, however, that the 330 mm long carriage is modestly sized, and hence, these are very respectable values. Future work will focus on modeling the pitch error as a function of motor coil/magnet interaction, and strategies will be developed to further reduce this error.

When considering the application of this design as an alternative to ballscrew systems, one must consider the total force required for the system, which includes process and acceleration loads. Many small machine tools or material handling applications end up requiring a linear motor with modest force requirements on the order of 500 N. Considering that a typical water-cooled linear electric motor can obtain an effective motor force/motor-forcer-area on the order of 30 kPa, this results in a modest sized motor forcer. Motor forcer length/width ratios are typically on the order of 4:1, so this means the motor force will be about 65 mm × 260 mm. However, if this design were to be applied to larger OD grinders with reciprocating wheel heads for grinding eccentrics, the forces required can be on the order of thousands of Newtons and are dominated by inertial loads; thus, it can be imperative to minimize the mass of moving components.

Acknowledgments

The authors would like to thank Andrew Devitt of New Way Bearings Inc. for supplying the porous carbon air bearings and for assistance in installing them; Anorad Corporation for their generous donation of the linear motor for the first test system; Gerry Parrot of Rock of Ages Corporation for manufacturing the granite; and Phil Greene of Dover Instrument Corporation for helping us integrate a controller with the motor and perform the metrology experiments. Overbeck Machine Tool of Long Island NY provided the resources for creating and testing the bench level prototype; and Jeff Roblee and Fred Mispel of Precitech Inc. of Keene, NH measured the parts that were ground on the bench level prototype. The authors would also like to thank Prof. David Trumper and Eric Varady for their editorial input. Dr. Layton Hale of LLNL provided valuable input on modeling issues associated with porous aerostatic bearings.

References

[1] Roe J. English and American Tool Builders, © 1916 Yale University Press; p. 99.
[2] Moore W. Foundations of mechanical accuracy, Moore Special Tool Co., 1800 Union Avenue, Bridgeport, CT 06607, 1970, p. 21–46.
[3] Bryan JB. Design and construction of an ultra precision 84 inch diamond turning machine. Precision Eng. 1(1);1979.
[4] Chitayat A. Workpiece positioning table with air bearing pads. US Patent 4,392,642, 12 July, 1983.
[5] Rasnick WH, et al. Porous graphite air-bearing components as applied to machine tools. SME Tech. Report MRR74-02.
[6] Van Deuren FH. Guiding device. US Patent 4,817,930, 9 November, 1987.
[7] Devitt A, Slocum A. Method for manufacturing externally pressurized bearing assemblies. US Patent 5,488,771, 6 February, 1996.
[8] Slocum AH, Scagnetti PE, Kane NR, Brünnner C. Design of self compensated water-hydrostatic bearings. Precision Eng 1995;17(3):173–85.
[9] Slocum AH. Linear motion carriage system and method with bearings preloaded by inclined linear motor with high attractive force. US Patent 6,150,740, November 2000.
[10] Slocum A, Basaran M, Cortesi R. Linear motion carriage with bearings preloaded by inclined open-face iron core linear electric motor. In: Proceedings of the European Society for precision engineering (EUSPEN) annual meeting, 27–30 May, 2002.
[11] Horikawa O, et al. Vibration, position, and stiffness control of an air journal bearing. In: Proceedings of the 1989 international precision engineering symposium, Monterey CA, p. 321–32.
[12] Zeleny J. Servostatic guideways—a new kind of hydraulically operating guideways for machine tools. In: Proceedings of the 10th international machine tool design research conference, September 1969.
[13] Tsumaki N, Tokisue H, Inoue H. Guiding apparatus. US Patent 4,630,942, 23 December, 1986.
[14] Marathe S, et al. Servostatic bearing system with variable stiffness. 4,080,009, 21 March, 1978.
[15] Degast J. Hydrostatic bearings. US Patent 3,442,560, May 6, 1969.
[16] Vemuri S, Fedder GK, Mukherjee T. Low order squeeze film model for simulation of MEMS devices. In: Proceedings of the 2000 international conference on modeling and simulation of microsystems MSM 2000, San Diego, CA, 27–29 March 2000.
[17] Senturia S. Microsystem design. Boston: Kluwer; 2000. p. 332–9.
[18] Veijola T, et al. Circuit simulation model of gas damping in microstructures with nontrivial geometries. In: Proceedings of Transducers ‘95, Stockholm, Sweden, 25–29 June, 1995; p. 36–40.
[19] Hays DF. Squeeze films for rectangular plates. Trans Am Soc Mech Eng, J Basic Eng, June 1963. p. 243–6.
[20] Fuller D. Theory and practice of lubrication for engineers. 2nd ed. New York: Wiley; 1984. p. 181–5.
[21] Slocum AH. Precision machine design. Eaglewood Cliffs, NJ: Prentice Hall; 1992.
[22] Frey D, Otto K, Pflager W. Swept envelopes of cutting tools in integrated machine and workpiece error budgeting. Ann CIRP 1997;46(1):475–80.
[23] Veijola T, Mattila T. Compact squeezed-film damping model for perforated surface. In: Proceedings of Transducers ‘01, München, Germany, 10–14 June 2001, p. 1506–9.